Structural Engineering and Mechanics, Vol. 15, No. 6 (2003) 653-668
DOI: http://dx.doi.org/10.12989/sem.2003.15.6.653

A study of the nonlinear dynamic instability of hybrid cable dome structures

Seung-Deog Kim†

Department of Architectural Engineering, Semyung University, Jecheon 390-711, Korea

Hyung-Seok Kim‡ and Moon-Myung Kang‡†

Department of Architectural Engineering, Kyungpook National University, Daegu 702-701, Korea

(Received August 10, 2001, Accepted March 22, 2003)

Abstract. Many papers which deal with the dynamic instability of shell-like structures under the STEP load have been published. But, there have been few papers related to the dynamic instability of hybrid cable domes. In this study, the dynamic instability of hybrid cable domes considering geometric nonlinearity is investigated by a numerical method. The characteristic structural behaviour of a cable dome shows a strong nonlinearity, so we determine the shape of a cable dome by applying initial stress and examine the indirect buckling mechanism under dynamic external forces. The dynamic critical loads are determined by the numerical integration of the nonlinear equation of motion, and the indirect buckling is examined by using the phase plane to investigate the occurrence of chaos.

Key words: hybrid structure; cable dome; indirect buckling; nonlinear; initial imperfection; phase plane; chaos.

1. Introduction

After civilization began, large space structures were in continuous demand, because human beings pursued life in larger and more affluent spaces. Changes in roof structures are the most important factor for the possibility of making large space structures (Makowski 1993). Roofs gradually lightened with the change of materials and technical developments, and the present technique can exceed a span of 300 meters.

Following such a trend, the construction of large space structures is rapidly increasing all over the world and accordingly, incidents of collapse are on the rise. To build safer and more economical buildings, we have to know the precise collapse mechanism of large space structures, and many researchers have focused on this problem (Kani and McConnel 1987, See and McConnel 1986). However, relatively many researchers have been studying the collapse mechanism by a static load, but there are few investigations into the collapse mechanism by dynamic external forces, and the

† Associate Professor
‡ Doctor's Course
‡† Professor

collapse mechanism by dynamic load is greatly different from a situation involving a static load (Hangai 1971, Holzer 1977).

A shape resistant shell structure is an extremely efficient mechanical creation because it transmits forces mainly by in-plane forces, but at a certain load level it changes from a stable condition to an unstable condition or vice versa. Therefore, it is very important to grasp the collapse mechanism due to the unstable phenomenon and we have to reflect it in the design process. The important aspect of the instability problem of a shell type structural system is that it reacts to the initial condition very sensitively, so the nonlinear analysis problem becomes very unstable and this is caused by the limitation of mathematics (Huang 1968, Hsu 1966, 1967, Yao 1991).

The structural instability problem can be divided into two classes. One class is the static instability problem and the other is the dynamic instability problem.

Since the announcement of the classical buckling load of spherical shells by Zoelly (1915), the static instability problem of shell type structures has been studied by many researchers, and the design standard is also provided (Huang 1964, Suhara 1960). However, research into the dynamic instability problem of shell type structures is insufficient (Kim 1995) because the numerical analysis of the nonlinear dynamic equation of motion is extremely difficult (Kouhia 1989, Waszczyszyn 1983).

The structural system that discreterized continuous shells is frequently used to make dome-type structures, and it is generally used to make large space structures because the weight is lightened and redundant force is increased. This kind of structure shows the instability phenomenon by snap-through or bifurcation according to the shape of structure, and the understanding of the collapse mechanism by this phenomenon is very important to the design process (Hill 1989, Lin 1990). In the case of the dynamic loading condition, the studies of the collapse mechanism by unstable phenomenon is still in the incipient stage (Coan 1983, Kim 1990, 1997). In the dynamic instability problem, snap-through corresponds to the direct buckling and bifurcation corresponds to the indirect buckling.

In this study, we shall investigate the dynamic instability phenomenon of the Geiger model, which is the most well known among the cable dome structures that is the lightweight hybrid structure using compression and tension element continuously. The structural behaviour of the cable dome shows a strong nonlinearity according to the initial stress and external forces. Therefore, we determine the shape by applying initial stress and then investigate the indirect buckling mechanism by the dynamic external forces.

First we obtain the static bifurcation buckling load by a static nonlinear analysis. With the static analytic results, we execute the dynamic nonlinear analysis and compare its results with the static bifurcation buckling load. We consider the nonlinear transient response and the characteristic of attractor in the phase plane to grasp the generation path of the dynamic buckling. Also, we investigate the generation of chaos in the indirect buckling, which is the dynamic nonlinear problem reacting sensitively by the initial imperfection.

2. Nonlinear stiffness equation of the cable element

Fig. 1 shows the element coordinates of nonlinear cable element in the local coordinate system.

The displacements within an element can be expressed in terms of the nodal displacements by using Lagrangian interpolation functions N_i and N_j.

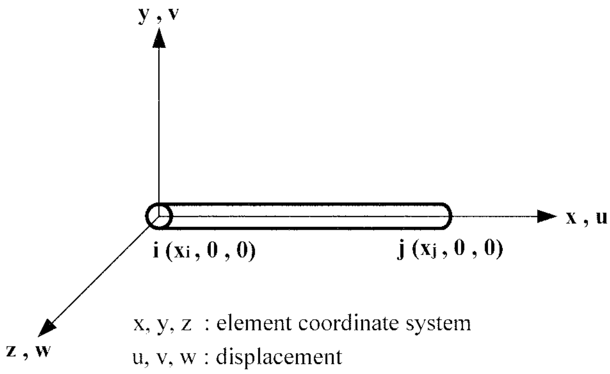

Fig. 1 Element coordinate system of cable element

$$\begin{aligned} u(x) &= N_i d_{xi} + N_j d_{xj} \\ v(x) &= N_i d_{yi} + N_j d_{yj} \\ w(x) &= N_i d_{zi} + N_j d_{zj} \end{aligned} \tag{1}$$

where,

$$N_i = 1 - \xi, \quad N_j = \xi, \quad \xi = \frac{x - x_i}{x_j - x_i} \tag{2}$$

The strain-displacement relationship of element is given as Eq. (3) including quadratic terms which means the geometric nonlinearity.

$$\varepsilon_x = \boldsymbol{A}_1 \boldsymbol{d} + \frac{1}{2} \boldsymbol{d}^T \boldsymbol{B}^T \boldsymbol{B} \boldsymbol{d} \tag{3}$$

Where,

$$\boldsymbol{A}_1 = [N_{i,x} \;\; 0 \;\; 0 \;\; N_{j,x} \;\; 0 \;\; 0]$$

$$\boldsymbol{d} = [d_{xi} \;\; d_{yi} \;\; d_{zi} \;\; d_{xj} \;\; d_{yj} \;\; d_{zj} \;\;]^T$$

$$\boldsymbol{B} = \begin{bmatrix} N_{i,x} & 0 & 0 & N_{j,x} & 0 & 0 \\ 0 & N_{i,x} & 0 & 0 & N_{j,x} & 0 \\ 0 & 0 & N_{i,x} & 0 & 0 & N_{j,x} \end{bmatrix} \tag{4}$$

The stress-strain relationship in the incremental section is given in Eq. (5).

$$\sigma_x = E\varepsilon_x \tag{5}$$

where, E is Young's modulus.

The virtual work equation of nonlinear cable element is given as,

$$\int_V \sigma_x \delta\varepsilon_x dV = \boldsymbol{f}^T \delta \boldsymbol{d} \tag{6}$$

Assuming the present state of things as an initial state and then applying the principal of virtual work, Eq. (6) can be written as Eq. (7).

$$\int_V [(\sigma_x^{(0)} + \sigma_x)\delta\varepsilon_x]dV = (\boldsymbol{f}^{(0)} + \boldsymbol{f})^T \delta\boldsymbol{d} \tag{7}$$

Substitute $\delta\varepsilon_x$ obtained from Eq. (3) to Eq. (7), then replace the volume integral with uniform area A and length l, Eq. (7) can be expressed as,

$$Al[(\sigma_x^{(0)} + \sigma_x)(\boldsymbol{A}_1 + \boldsymbol{d}^T\boldsymbol{B}^T\boldsymbol{B})]\delta\boldsymbol{d} = (\boldsymbol{f}^{(0)} + \boldsymbol{f})^T \delta\boldsymbol{d} \tag{8}$$

As the $\delta\boldsymbol{d}$ of Eq. (8) is virtual displacement, so for non-trivial solution,

$$Al[(\sigma_x^{(0)} + \sigma_x)(\boldsymbol{A}_1 + \boldsymbol{d}^T\boldsymbol{B}^T\boldsymbol{B})] = (\boldsymbol{f}^{(0)} + \boldsymbol{f})^T \tag{9}$$

Replace ε_x of Eq. (5) with Eq. (3) and then substitute to Eq. (9),

$$(\boldsymbol{f}^{(0)} + \boldsymbol{f})^T = Al\left\{\left(\sigma_x^{(0)} + E\boldsymbol{A}_1\boldsymbol{d} + \frac{1}{2}E\boldsymbol{d}^T\boldsymbol{B}^T\boldsymbol{B}\boldsymbol{d}\right)(\boldsymbol{A}_1 + \boldsymbol{d}^T\boldsymbol{B}^T\boldsymbol{B})\right\} \tag{10}$$

Eliminate over quadratic terms to $\boldsymbol{d}$ and transpose both sides, Eq. (10) can be written as,

$$\boldsymbol{f}^{(0)} + \boldsymbol{f} = Al(\boldsymbol{A}_1^T\sigma_x^{(0)}) + Al(\sigma_x^{(0)}\boldsymbol{B}^T\boldsymbol{B})\boldsymbol{d} + AlE(\boldsymbol{A}_1^T\boldsymbol{A}_1)\boldsymbol{d} + \text{higher order terms} \tag{11}$$

In Eq. (11), we define the residual force caused by eliminating higher order terms to $\boldsymbol{d}$ as,

$$\boldsymbol{r} = Al\boldsymbol{A}_1^T\sigma_x^{(0)} - \boldsymbol{f}^{(0)} \tag{12}$$

Using Eq. (12), Eq. (11) can be expressed as,

$$\boldsymbol{f} - \boldsymbol{r} = AlE(\boldsymbol{A}_1^T\boldsymbol{A}_1)\boldsymbol{d} + Al(\sigma_x^{(0)}\boldsymbol{B}^T\boldsymbol{B})\boldsymbol{d} \tag{13}$$

where,

$\boldsymbol{k}_E = AlE(\boldsymbol{A}_1^T\boldsymbol{A}_1)$: Elastic stiffness matrix

$\boldsymbol{k}_G = Al(\sigma_x^{(0)}\boldsymbol{B}^T\boldsymbol{B})$: Geometric stiffness matrix

The nodal load vector, residual force vector and nodal displacement vector in the local coordinate system can be written to the value of global coordinate system by using transformation matrix $\boldsymbol{T}$.

$$\boldsymbol{f} = \boldsymbol{TF}, \quad \boldsymbol{r} = \boldsymbol{TR}, \quad \boldsymbol{d} = \boldsymbol{TD} \tag{14}$$

So, Eq. (13) can be written as,

$$\boldsymbol{T}(\boldsymbol{F} - \boldsymbol{R}) = [\boldsymbol{k}_E + \boldsymbol{k}_G]\boldsymbol{TD} \tag{15}$$

Therefore, the tangent stiffness matrix in the global coordinate system can be obtained as Eq. (16).

$$\boldsymbol{F} - \boldsymbol{R} = [\boldsymbol{K}_E + \boldsymbol{K}_G]\boldsymbol{D} \tag{16}$$

where,

$$\boldsymbol{K}_E = \boldsymbol{T}^T \boldsymbol{k}_E \boldsymbol{T} \text{ : Elastic stiffness matrix in the global coordinate system}$$

$$\boldsymbol{K}_G = \boldsymbol{T}^T \boldsymbol{k}_G \boldsymbol{T} \text{ : Geometric stiffness matrix in the global coordinate system}$$

3. Analytic model

To examine the dynamic instability phenomenon of hybrid structures, we adopted the Geiger-type cable dome, which is frequently used to make large space structures in recent years. This model has excellent structural efficiency, but it possesses the danger of collapse by in-plane twist because of its lightweight and flexibility.

Fig. 2 shows the node and element number of an analytic model and Table 1 is the nodal coordinates. Material properties of each element are, Young's modulus $E = 1.6 \times 10^6$ kgf/cm^2,

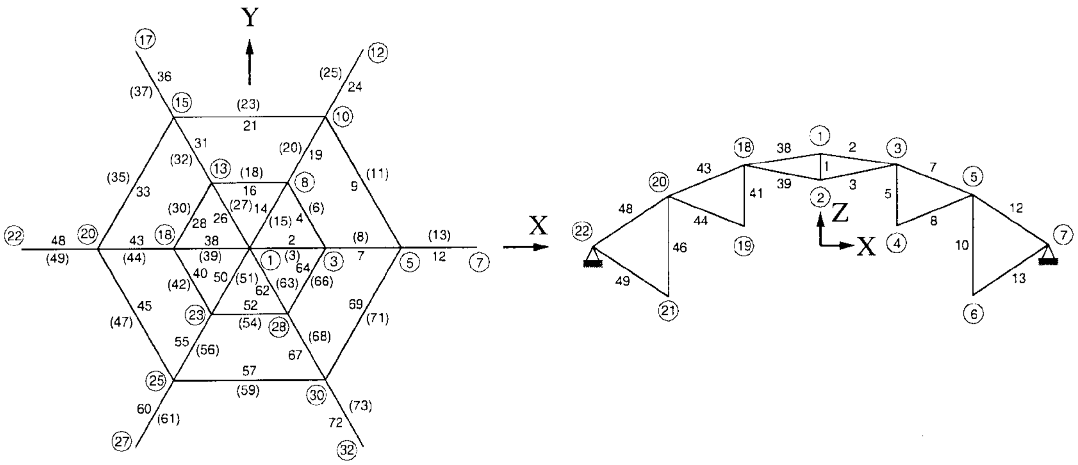

(a) Plan (b) Cross Section

Fig. 2 Analytic model

Table 1 Nodal coordinates (unit : cm)

Node number	1	2	3	4	5	6	7
X - coordinate	0.0	0.0	20.0	20.0	40.0	40.0	60.0
Z - coordinate	21.0	15.0	18.5	4.50	11.5	–11.5	0.0

Table 2 Cross section of element (unit: cm^2)

Element number	1	2	3	4	5	6	7
Cross section	1.00	0.01	0.01	0.01	1.00	0.02	0.02
Element number	8	9	10	11	12	13	
Cross section	0.02	0.01	1.00	0.04	0.04	0.04	

density $\rho = 7.85 \times 10^{-3}$ kgf/cm^3, and Table 2 is the cross section. The boundary condition of external nodes 7, 12, 17, 22, 27, 32 are clamped and the others are free.

We used two kinds of load modes, as shown in Fig. 3. Symbol ● represents the node where the load is acting to the –Z-direction. A-type is the total axisymmetrical load model and B-type is the partial axisymmetrical load model.

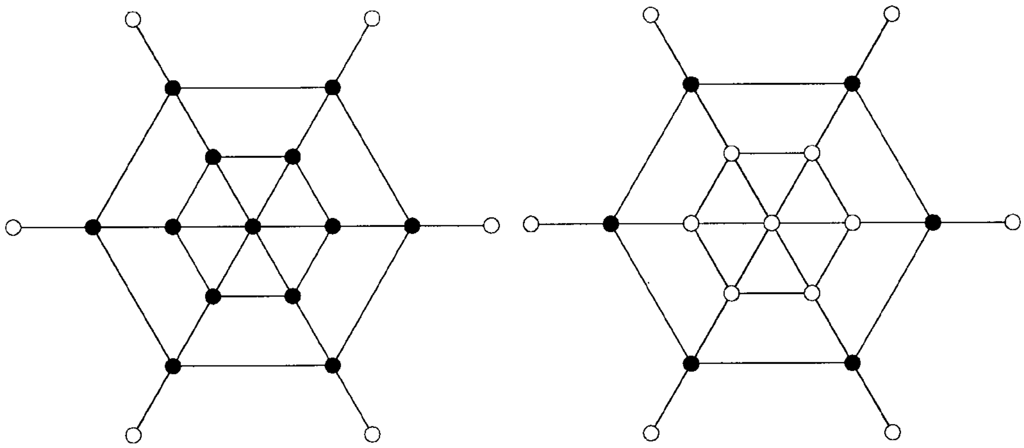

(a) Total axisymmetrical load model (A-Type) (b) Partial axisymmetrical load model (B-Type)

Fig. 3 Load mode

Cable dome is initially unstable, therefore we have to apply initial stress for the stabilization of the structure (Lin 1990, Kwun 1995). The initial stress is the value at the equilibrium state by performing the shape analysis, and Fig. 4 shows the values of initial stresses.

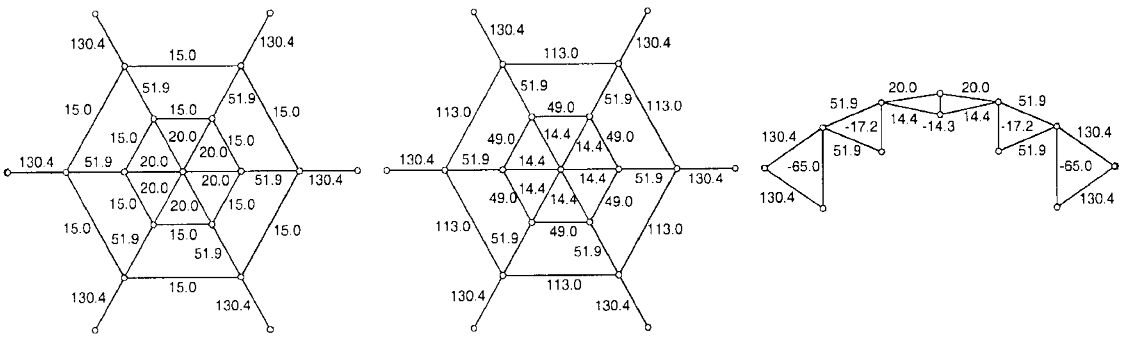

(a) Upper string plan (b) Lower string plan (c) Cross Section

Fig. 4 Initial stress (unit : kgf)

4. Numerical results and discussions

4.1 Static nonlinear instability analysis

To examine the bifurcation phenomenon in the static instability analysis, we have to introduce an initial imperfection. Initial imperfection is chosen from the first eigen vector which is obtained by eigen value analysis at the initial increment of tangent stiffness matrix, and we regarded it as an initial imperfection mode. Fig. 5 is the initial imperfection mode, where the solid line indicates the upper element and the dotted line indicates the lower element.

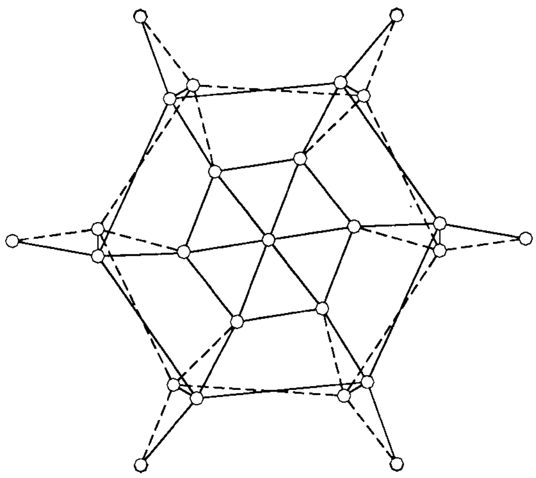

Fig. 5 Initial imperfection mode

In this study, we choose the magnitude of the initial imperfection as 0.01% and 0.1% of the span, and the analytic results are compared with that of the perfectly shaped model.

As the static nonlinear analytic method, we trace the critical load according to step by step analysis using the tangent stiffness equation of Chapter 2. Here, we used the displacement incremental method, that is, incrementing the displacement of node #1 to −Z-direction by 0.01 cm and compute the load factor and determinant of tangent stiffness matrix at each step.

Fig. 6 shows the determinants of the tangent stiffness matrix which are normalized by the initial determinant. In this figure, the solid line denotes the perfectly shaped model and the dotted lines represent the model has initial imperfection of 0.01% and 0.1%, respectively.

In case of the prefectly shaped model, the point that the determinant curves pass through zero line is 11.9 kgf (total load is 154.7 kgf) per node for A-type and 43.35 kgf (total load is 260.1 kgf) per node for B-type, respectively. These values are the static critical loads.

But, in cases of initially imperfected models, the determinant curves do not pass through zero line and this phenomenon is clearer when the magnitude of initial imperfection is larger. Because the perfectly shaped model can not avoid the unstable point, the determinant curves have to pass through the zero line, but by applying initial imperfection, the rigidity becomes stabilized state rapidly after the critical load level. That is, the main displacement modes are coupling with a new independent buckling mode as load level approaches close to the critical load level. Moreover, the

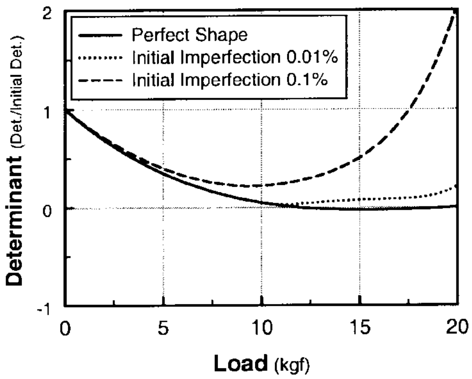

(a) A-Type

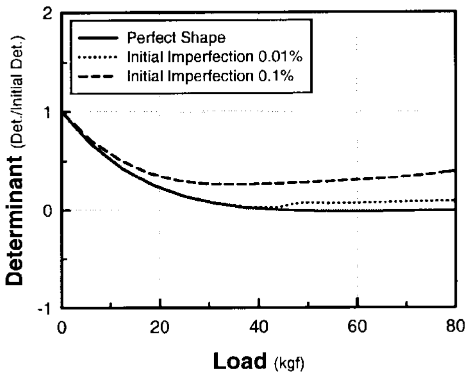

(b) B-Type

Fig. 6 Determinant curves

magnitude of initial imperfection becomes larger, the stabilization of rigidity becomes more rapid and this phenomenon is clearer in A-type than B-type.

Therefore, we can know that the instability phenomenon of this Geiger-type cable dome is generated by the bifurcation.

4.2 Nonlinear dynamic instability analysis

We used the Newmark's direct integration method to obtain the nonlinear dynamic responses of cable dome. In this study, we obtain the displacement vector at time $t + \Delta t$ and using this, calculate the velocity vector and acceleration vector. And replace the values at time $t + \Delta t$ with the values at time t, then compute increasing time increment Δt in succession. At this time, we obtain the nodal coordinates and element forces newly at each step and using this renew the geometric stiffness matrix of the following step.

Load mode for nonlinear dynamic instability analysis is limited to A-type and load condition is the vertical STEP function excitation. And we used load parameter α, which is normalized by static critical load 11.9 kgf. That is, $\alpha = 1$ means the static critical load level.

We obtained the dynamic nonlinear responses at each load level and graph the maximum displacement of each load level. At this time, time increment Δt is 1/100 of first natural period T_1 and duration is $10T_1$. For this model, T_1 is 1.3196 sec. When we obtain the dynamic response considering geometric nonlinearity, the critical load and displacement response is changed a little by the change of time increment Δt. But previous research has studied there is not a big difference to the decisive critical load (Kim 1990).

Fig. 7 shows the maximum displacement responses of node #3 and #5. From this figure, the perfectly shaped model does not reveal nonlinear phenomenon, but the initially imperfected models reveal nonlinear effect strongly. That is, the displacements diverge when the load level exceeds $\alpha = 0.76$ in the case of 0.01% initial imperfection and $\alpha = 0.58$ in the case of 0.1% initial imperfection. As you can know from the Y-direction graph, according to the load level increases the unstable phenomenon is happened by in-plane twist and consequently the displacements increase rapidly, so the displacements of X- and Z-direction diverge together.

This phenomenon is the indirect buckling which is correspond to the bifurcation in the static

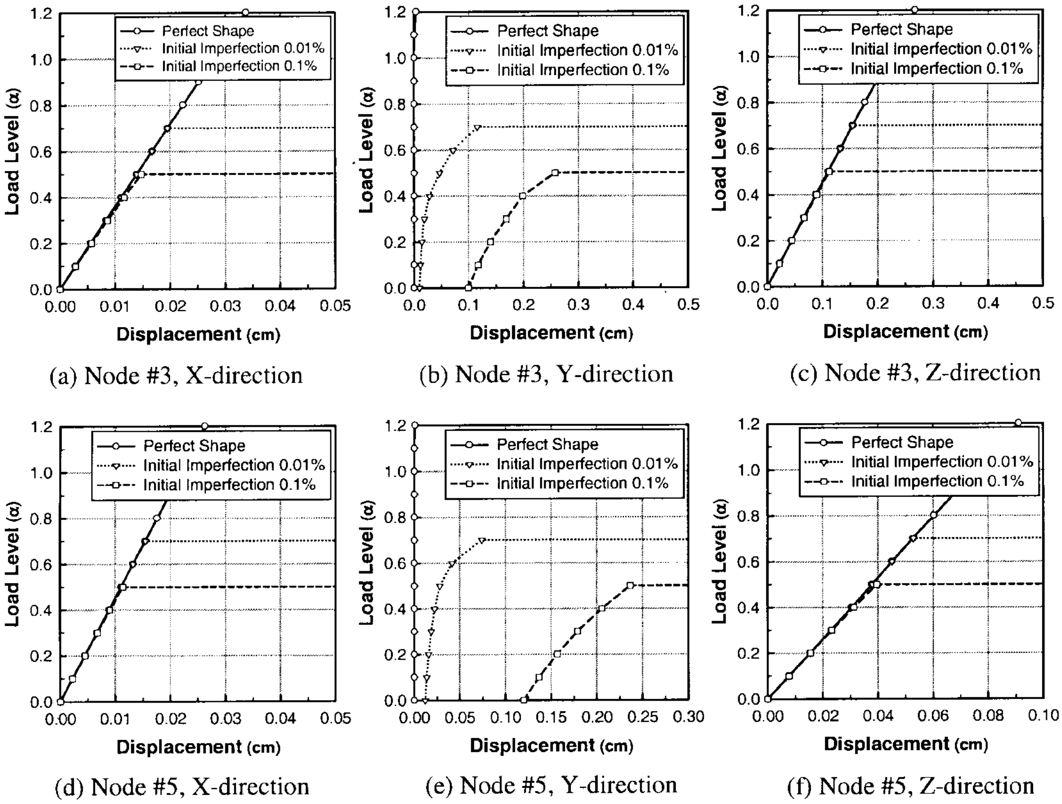

Fig. 7 Maximum dynamic displacement responses

buckling. Therefore, the collapse mechanism of Geiger-type cable dome is formed by indirect buckling caused by in-plane twist, and the critical load level is greatly dependent to the magnitude of initial imperfection.

The Geiger-type model used in this study, the dynamic critical load is lowerd to 50-80% of the static one.

We can understand this mechanism in detail by analyzing the displacement responses.

Fig. 8 and Fig. 9 are the displacement responses of node #3 and #4 with perfectly shaped model and load level α = 1.0. The Y-direction displacement responses are nearly zero, so the in-plane twist buckling cannot happen. The X- and Z-direction displacements are vibrating with the same cycle.

In case of 0.01% initial imperfection, dynamic buckling is occurred in the vicinity of α = 0.76. So we examined the displacement responses of pre-buckling load level α = 0.76 and post-buckling load level α = 0.77. Fig. 10 and Fig. 11 show the displacement responses of node #3 with load level α = 0.76 and 0.77, respectively. And Fig. 12 and Fig. 13 are the displacement responses of node #5 with load level α = 0.76 and α = 0.77.

In case of 0.1% initial imperfection, dynamic buckling is happened near α = 0.58. So the displacement responses of pre-buckling load level α = 0.58 and post-buckling load level α = 0.59 are examined. The results of node #3 with α = 0.58 and α = 0.59 are shown in Fig. 14 and Fig. 15, and the results of node #5 are shown in Fig. 16 and Fig. 17, respectively.

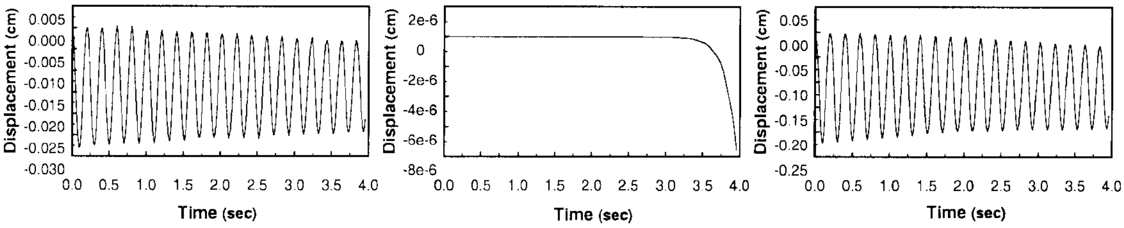

(a) X-direction (b) Y-direction (c) Z-direction

Fig. 8 Displacement responses of perfect shape (Node #3)

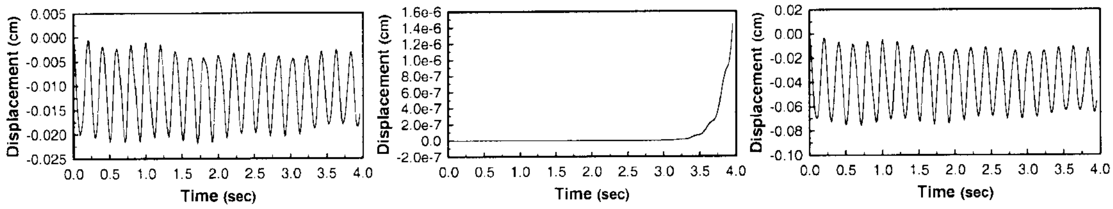

(a) X-direction (b) Y-direction (c) Z-direction

Fig. 9 Displacement responses of perfect shape (Node #5)

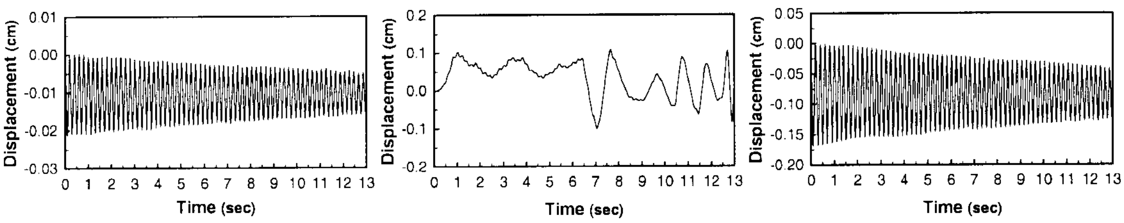

(a) X-direction (b) Y-direction (c) Z-direction

Fig. 10 Displacement responses of 0.01% initial imperfection (Node #3, α = 0.76)

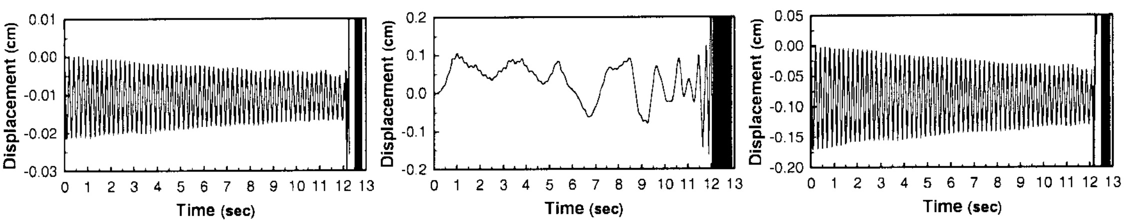

(a) X-direction (b) Y-direction (c) Z-direction

Fig. 11 Displacement responses of 0.01% initial imperfection (Node #3, α = 0.77)

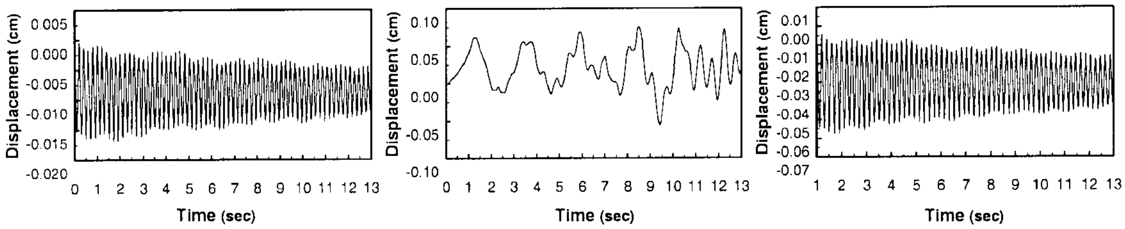

(a) X-direction (b) Y-direction (c) Z-direction

Fig. 12 Displacement responses of 0.01% initial imperfection (Node #5, α = 0.76)

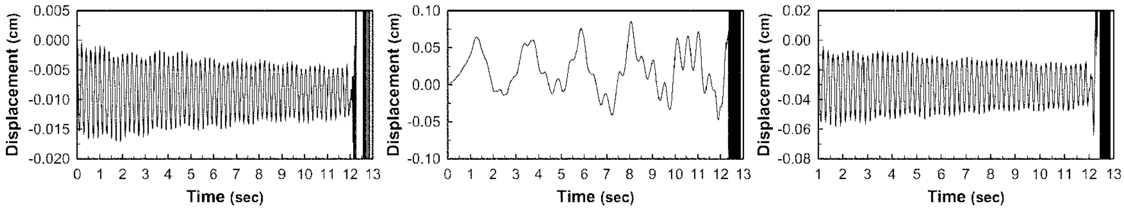

(a) X-direction (b) Y-direction (c) Z-direction

Fig. 13 Displacement responses of 0.01% initial imperfection (Node #5, α = 0.77)

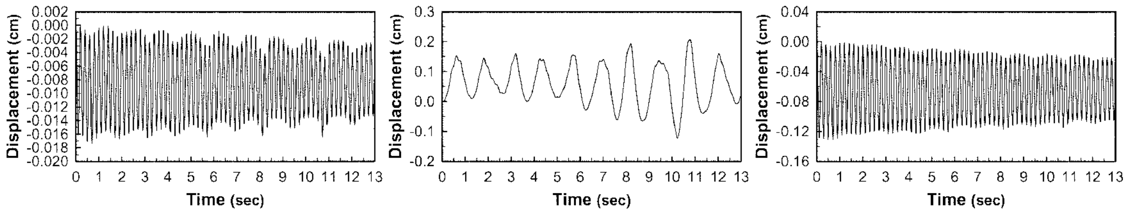

(a) X-direction (b) Y-direction (c) Z-direction

Fig. 14 Displacement responses of 0.1% initial imperfection (Node #3, α = 0.58)

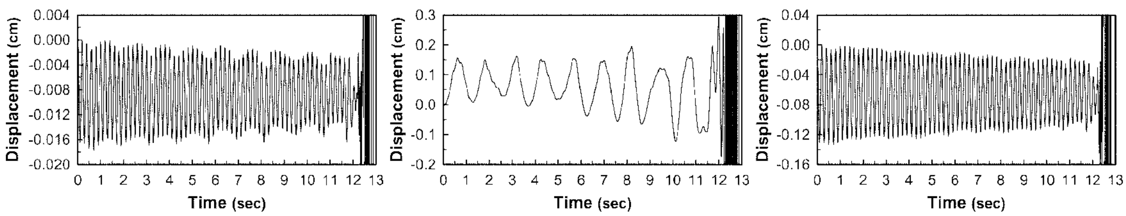

(a) X-direction (b) Y-direction (c) Z-direction

Fig. 15 Displacement responses of 0.1% initial imperfection (Node #3, α = 0.59)

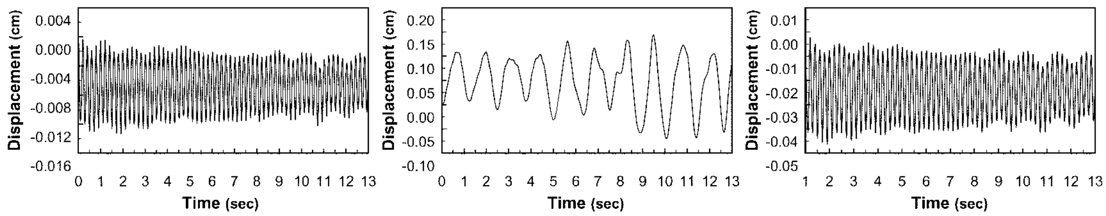

(a) X-direction (b) Y-direction (c) Z-direction

Fig. 16 Displacement responses of 0.1% initial imperfection (Node #5, α = 0.58)

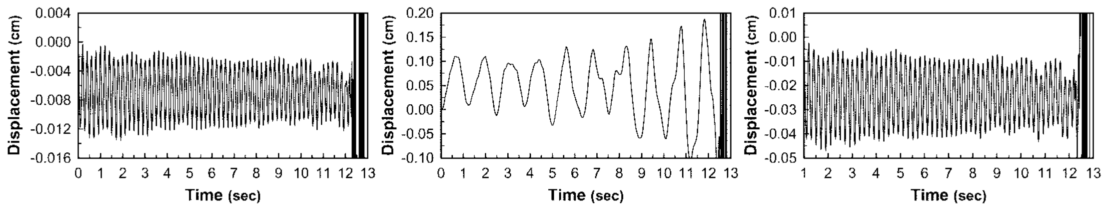

(a) X-direction (b) Y-direction (c) Z-direction

Fig. 17 Displacement responses of 0.1% initial imperfection (Node #5, α = 0.59)

We can find out from these figures, especially in Y-direction responses, that the responses of pre-buckling load level reveal the normal transient responses, but in case of post-buckling load level reveals a divergence after 11 seconds. This phenomenon is occurred by the indirect buckling which is happened from the coupling between main deformation modes and an independent buckling mode.

We analyzed the phase plane near the dynamic critical load level to examine the dynamic instability phenomenon of cable dome.

Fig. 18 and Fig. 19 show the phase planes of node #3 and #5 in case of perfectly shaped model. In the orbit of phase planes of X- and Z-direction, the attractor shows the torus, which is moving continuously and more than two limit cycles are maintaining independence. But, Y-direction attractor is very weak and progressing individual path.

In case of 0.01% initial imperfection, we examined the phase planes of pre-buckling load level α = 0.76 and post-buckling load level α = 0.77. Fig. 20 and Fig. 21 show the phase planes of node #3 with load level α = 0.76 and α = 0.77, respectively. Fig. 22 and Fig. 23 are the phase planes of node #5 with load level α = 0.76 and α = 0.77.

In case of 0.1% initial imperfection, the phase planes of pre-buckling load level α = 0.58 and post-buckling load level α = 0.59 is examined. The results of node #3 with α = 0.58 and α = 0.59 are shown in Fig. 24 and Fig. 25, and the results of node #5 are shown in Fig. 26 and Fig. 27, respectively.

From these figures, we can know that X- and Z-direction curves represent the torus, in which more than two limit cycles are in motion independently, similar to the perfectly shaped model. But, the Y-direction attractor reveals a chaotic behaviour forming a strange attractor, which is a non-overlapping new orbit caused by amplification of nonlinearity. And, as the magnitude of initial imperfection becomes larger, the characteristic of attractor becomes clearer.

Therefore, it is a chaotic phenomenon sensitive to the initial condition.

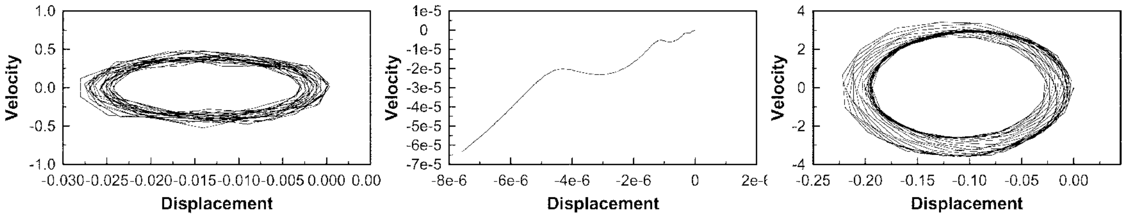

(a) X-direction (b) Y-direction (c) Z-direction

Fig. 18 Phase plane of perfect shape (Node #3)

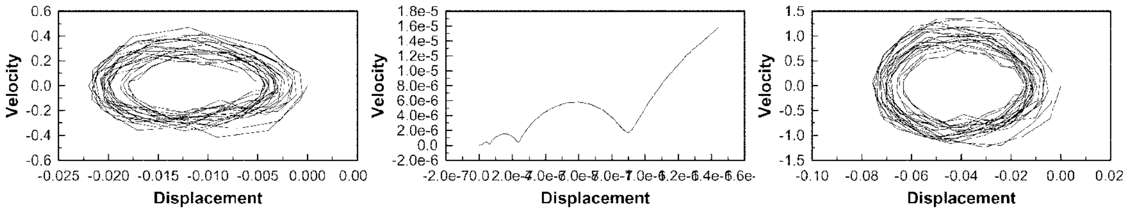

(a) X-direction (b) Y-direction (c) Z-direction

Fig. 19 Phase plane of perfect shape (Node #5)

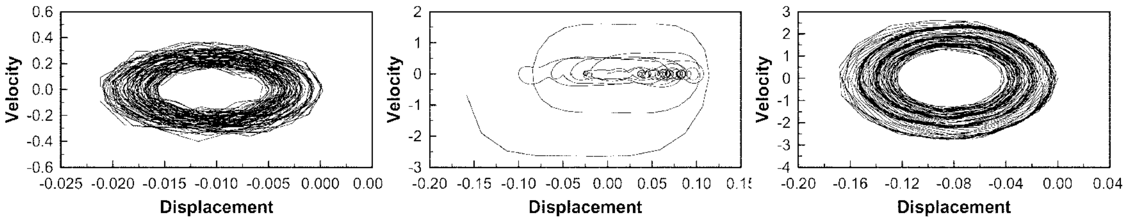

(a) X-direction (b) Y-direction (c) Z-direction

Fig. 20 Phase plane of 0.01% initial imperfection (Node #3, α = 0.76)

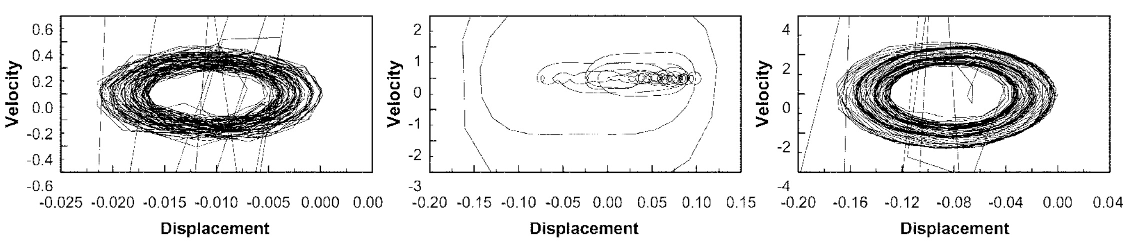

(a) X-direction (b) Y-direction (c) Z-direction

Fig. 21 Phase plane of 0.01% initial imperfection (Node #3, α = 0.77)

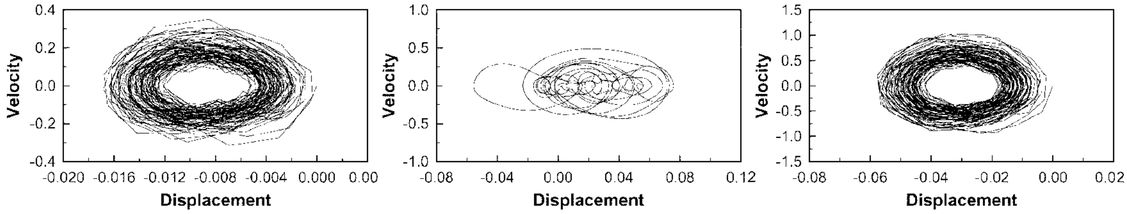

(a) X-direction (b) Y-direction (c) Z-direction

Fig. 22 Phase plane of 0.01% initial imperfection (Node #5, α = 0.76)

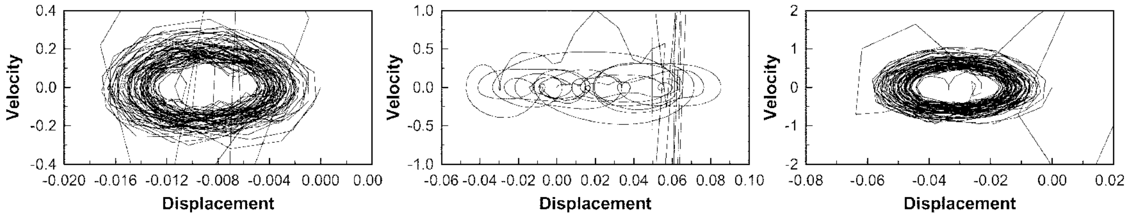

(a) X-direction (b) Y-direction (c) Z-direction

Fig. 23 Phase plane of 0.01% initial imperfection (Node #5, α = 0.77)

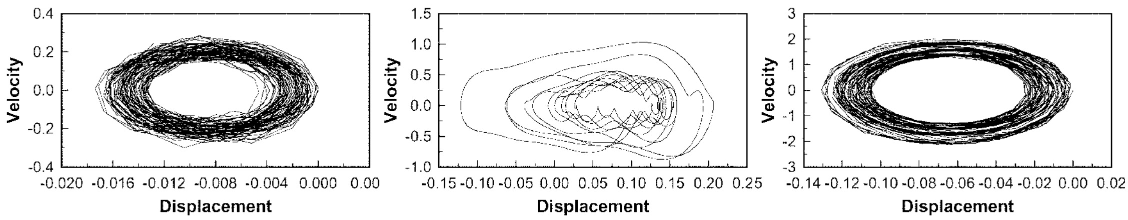

(a) X-direction (b) Y-direction (c) Z-direction

Fig. 24 Phase plane of 0.1% initial imperfection (Node #3, α = 0.58)

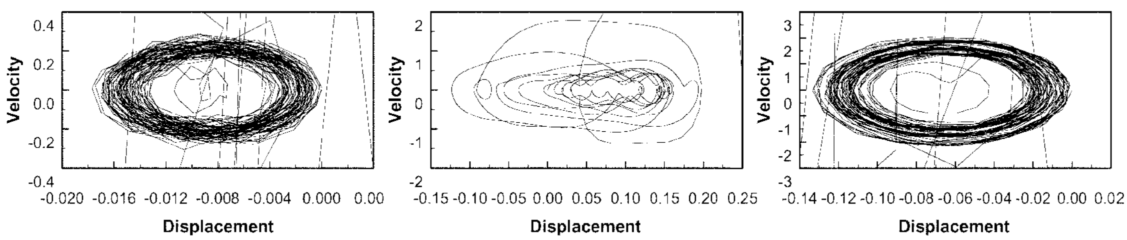

(a) X-direction (b) Y-direction (c) Z-direction

Fig. 25 Phase plane of 0.1% initial imperfection (Node #3, α = 0.59)

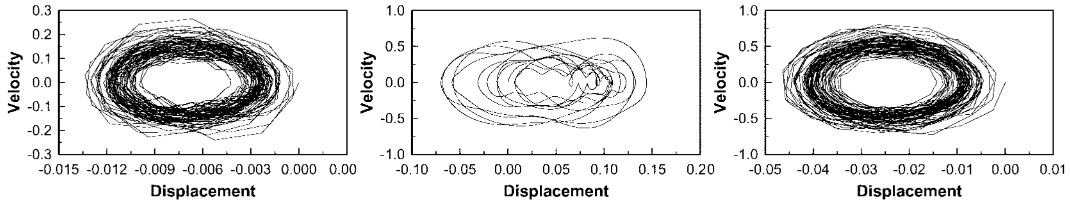

(a) X-direction (b) Y-direction (c) Z-direction

Fig. 26 Phase plane of 0.1% initial imperfection (Node #5, α = 0.58)

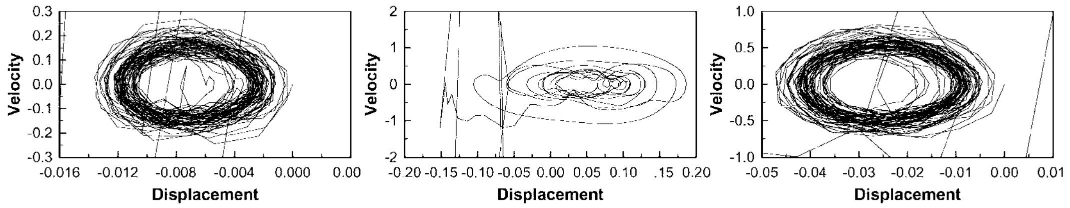

(a) X-direction (b) Y-direction (c) Z-direction

Fig. 27 Phase plane of 0.1% initial imperfection (Node #5, α = 0.59)

5. Conclusions

In this study, we examined the dynamic instability phenomenon of Geiger model, which is most well known among the large space structural systems.

First, we obtainined the static bifurcation buckling load by nonlinear static analysis. On the basis of the static analysis results, we executed the nonlinear dynamic analysis and compared it with the static bifurcation buckling load. And to grasp the generation path of the dynamic buckling, we examined the nonlinear transient responses and the characteristic of attractor in the phase plane. Also, we investigated the generation of chaos about the indirect buckling, which is the dynamic nonlinear problem react sensitively by the initial imperfection.

And the followings are observed.

1) The mechanism of dynamic instability for cable dome is happened by the divergence of displacement responses which is formed the coupling between main deformation modes and an independent orthogonal buckling mode.
2) The instability of Geiger-type cable dome is happened by the in-plane twist which is a kind of the bifurcation buckling, and therefore this phenomenon is the indirect buckling in dynamic responses.
3) Under the step function excitation, the dynamic buckling loads for the case of no damping are reduced about 50-80% of the static one.
4) The Geiger-type hybrid cable dome shows a chaotic behaviour in nonlinear dynamic analysis with initial imperfections.

Therefore, the collapse mechanism of Geiger-type hybrid cable dome is formed by the indirect buckling due to in-plane twist, and the critical load level is greatly sensitive to the maginitude of initial imperfections.

References

Coan, C.H. and Plaut, R.H. (1983), "Dynamic stability of a lattice dome", *Earthq. Eng. Struct. Dyn.*, **11**, 269-274.

Hangai, Y. and Kawamata, S. (1971), "Nonlinear analysis of space frames and snap-through buckling of reticulated shell structures", *Proceedings of IASS Pacific Symposium, Part II on Tension Structure and Space Frames*, Tokyo and Kyoto, Japan, 9-4-1 - 9-4-12.

Hill, C.D., Blandford, G.E. and Wang, S.T. (1989), "Post-buckling analysis of steel space trusses", *J. Struct. Eng.*, ASCE, **115**(4), 900-919.

Holzer, S.M. (1977), "Static and dynamic stability of reticulated shells : Stability of structures under static and dynamic loads", *Proceedings of an International Colloquium*, Washington, D.C., May.

Hsu, C.S. (1966), "On dynamic stability of elastic bodies with prescribed initial conditions", *Int. J. Eng. Sci.*, **4**(1), 1-21.

Hsu, C.S. (1967), "The effects of various parameters on the dynamic stability of a shallow arch", *J. Appl. Mech.*, **34**(2), 349-358.

Huang, N.C. (1964), "Unsymmetrical buckling of thin shallow spherical shells", *J. Appl. Mech.*, **31**(3), 447-457.

Huang, N.C. and Nachbar, W. (1968), "Dynamic snap-through of imperfect viscoelastic shallow arches", *J. Appl. Mech.*, ASME, 289-296.

Kani, I.M. and McConnel, R.E. (1987), "Collapse of shallow lattice domes", *J. Struct. Eng.*, **113**(8), 1806-1819.

Kim, S.D. (1990), "Dynamic instability of shallow structures", Doctorate thesis, The University of Tokyo.

Kim, S.D. (1995), "Spectral analysis of nonlinear dynamic response for dynamic instability of shallow elliptic paraboloidal shells", *J. Computational Structural Engineering Institute*, **8**(2), 153-161.

Kim, S.D., *et al*. (1997), "Dynamic instability of shell-like shallow trusses considering damping", *Comput. Struct.*, **64**(1-4), 481-489.

Kim, S.D., Kwun, T.J. and Park, J.Y. (1998), "A study on the bifurcation buckling for shallow sinusoidal arches", *J. Computational Structural Engineering Institute of Korea*, **11**(1), 457-464.

Kim, S.D., Park, J.Y. and Kwun, T.J. (1998), "A study on the instability of shallow sinusoidal arches", *J. Computational Structural Engineering Institute of Korea*, **11**(2), 233-242.

Kouhia, R. and Mikkola, M. (1989), "Tracing the equilibrium path beyond simple critical points", *Int. J. Numer. Meth. Eng.*, **28**(12), 2933-2941.

Kwun, T.J., Hangai, Y., Choi, H.S., Kim, S.D. and Seo, S.Y. (1995), "A study for optimum shape and stress-deformation analysis of cable net structures considering geometric nonlinearity", *Journal of Architectural Institute of Korea*, **111**(1), 153-160.

Lin, X.G. (1990), "Structural stability analysis of hybrid cable structures", Master's thesis, University of Tokyo.

Makowski, Z.S. (1993), "Space structures - a review of the development within the last decade", *Proc. 4th Int. Conf. Space Structures*, UK, September.

Nayfeh, A.H. and Mook, D.T. (1979), *Nonlinear Oscillations*, John Wiley & Sons.

See, T. and McConnel, R.E. (1986), "Large displacement elastic buckling of space structure", *J. Struct. Eng.*, **112**(5), 1052-1069.

Suhara, J. (1960), *Snapping of Shallow Spherical Shells under Static and Dynamic Loadings*, ASRL TR 76-4, Aeroelastic and Structures Research Laboratory, Cambridge, Mass.

Waszczyszyn, Z. (1983), "Numerical problems of nonlinear stability analysis of elastic structures", *Comput. Struct.*, **17**(1), 13-24.

Yao, J. and Song, B. (1991), "The dynamic elastic buckling of a circular arch with finite displacements and initial imperfections", *Int. J. Impact Eng*., **11**(4), 503-513.

Zoelly, R. (1915), "Ueber ein knickungsproblem an der kugelschale", Dissertation, Zurich.